AIP | Applied Physics Letters

Polarization- and angle-dependent characteristics in two dimensional photonic crystal membrane reflectors

Arvinder Singh Chadha, Deyin Zhao, Santhad Chuwongin, Zhenqiang Ma, and Weidong Zhou

Citation: Applied Physics Letters **103**, 211107 (2013); doi: 10.1063/1.4832221
View online: http://dx.doi.org/10.1063/1.4832221
View Table of Contents: http://scitation.aip.org/content/aip/journal/apl/103/21?ver=pdfcov
Published by the AIP Publishing

Polarization- and angle-dependent characteristics in two dimensional photonic crystal membrane reflectors

Arvinder Singh Chadha,[1] Deyin Zhao,[1] Santhad Chuwongin,[1] Zhenqiang Ma,[2] and Weidong Zhou[1,a)]
[1]*Department of Electrical Engineering, NanoFAB Center, University of Texas at Arlington, Texas 76019, USA*
[2]*Department of Electrical and Computer Engineering, University of Wisconsin-Madison, Wisconsin 53706, USA*

(Received 16 September 2013; accepted 5 November 2013; published online 19 November 2013)

We report here measured angle- and polarization-dependent reflection properties in two-dimensional photonic crystal broadband membrane reflectors. Polarization independent reflection was obtained at surface normal direction. High reflection can also be obtained for one transverse electric (TE) polarization state over a wide range of incident angles. With the target of 1550 nm spectral band, the measured spectral bandwidths for TE polarization with reflectivity greater than 90% are 180 nm and 56 nm at surface normal and oblique incidence of 45°, respectively. The experimental spectrum approximates the theoretical spectral response of this membrane reflector. © *2013 AIP Publishing LLC*. [http://dx.doi.org/10.1063/1.4832221]

Over the last few years, significant research progresses have been made in the area of single layer dielectric membrane reflectors (MR), based on one-dimensional (1D) high contrast gratings (HCG)[1–5] or two-dimensional (2D) photonic crystal slabs (PCS).[6–12] Due to the nature of the different mechanisms in these nano-structured dielectric MRs, as compared to the reflection principles in metallic reflectors and widely used multi-layer stacked distributed Bragg reflectors (DBR), it is very important to understand the angle- and polarization-dependent reflection properties.[6,7] These properties can also be engineered by dispersion engineering of the modal properties for the desired angle- and polarization-dependent properties. 1D grating structures are intrinsically polarization-dependent. Various structures have been proposed in 1D HCG broadband reflection structures for TE (transverse electric) only, TM (transverse magnetic) only, or both TE and TM polarized light.[13,14] Low birefringence in hollow core waveguides and broadband reflectors have also been reported in 1D HCGs.[15,16] On the other hand, 2D PCS based MRs can be intrinsically polarization independent, due to the high symmetry properties.[6,7] Lousse *et al.* provided detailed theoretical investigations on angle- and polarization-dependent characteristics in 2D PCS membrane reflectors.[6] Boutami *et al.* presented a design of 2D suspended InP PCS with a polarization independent reflection of ~250 nm bandwidth with reflectivity greater than 90% by exploiting two resonant waveguided modes at surface normal incidence.[7] We have reported earlier polarization independent reflections in a demonstrated MR on a glass substrate for surface-normal incident light.[9,10]

In this paper, we report detailed design and first experimental investigation of angle- and polarization-dependent reflection properties in 2D PCS based membrane reflectors on silicon on insulator (SOI) substrate. Shown in Fig. 1 are the schematic and the scanning electron micrograph (SEM) of the membrane reflector under study. The incident beam direction is defined by two polar angles, the colatitude angle θ (angle from the surface-normal direction) and the azimuth angle Φ (angle from the positive x-axis to the orthogonal projection of the incident beam in the x-y plane). The incident beam polarization (E-vector) Ψ is defined as the angle from the positive x-axis to the polarization direction. The TE (s) or TM (p) polarizations are defined as the beam with E-vector perpendicular or parallel to the incident plane formed by the incident and reflected light. The conventional definition of wave vector directions and the corresponding Brillouin zone in k-space with high symmetric points defined with Γ, X, and M, respectively, are also shown in Fig. 1. The reflector was designed using Rigorous Coupled Wave Analysis (RCWA) simulations,[17] with target wavelength around 1550 nm. The MR consists of 340 nm thick top Si with square lattice photonic crystal structure. The lattice constant (a) of the photonic crystal is 860 nm with the ratio of air hole radius to the lattice constant (r/a) of 0.45. It is possible to shift the spectral bandwidth and location of the reflection band by changing the geometric parameters of the reflector.

The simulated reflection spectra contour plots as a function of the incident angle are shown in Figs. 2(a) and 2(c) and Figs. 2(b) and 2(d) for TE and TM polarizations, respectively. In Figs. 2(a) and 2(b), the incident beam angle is changed from surface normal ($\theta = 0°$) to $\theta = 80°$ in steps of 10° and $\Phi = 0°$. At surface normal incidence, simulated specular bandwidth of 104 nm (1472 nm–1576 nm) with reflection greater than 95% is observed for both the TE and TM polarizations. However, with the increase of incident angle, broadband high reflectivity can only be observed for TE polarizations. The TM polarization reflectivity reduced drastically with the increase of the incident angle. To better understand this phenomenon, we did a fine scan to simulate the reflectivity at small incident angles from 0° to 15°. The results are shown in Figs. 2(c) and 2(d). When the incident angle (θ) is increased from 0° to 8°, reflectivity greater than 95% is maintained for both TE (Fig. 2(c)) and TM

a)wzhou@uta.edu

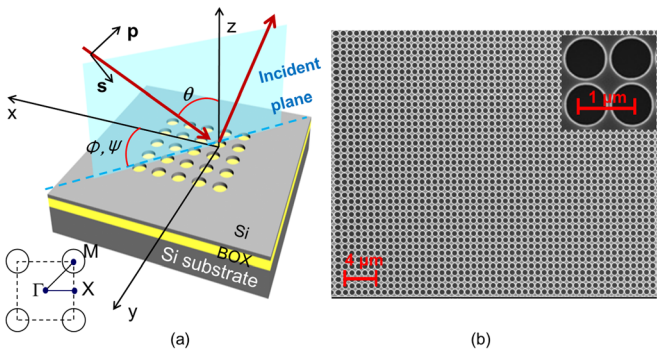

FIG. 1. (a) Schematic of the broadband membrane reflector with the angular and polarization definition of the incident light. (b) SEM images of the fabricated Si MR on SOI.

(Fig. 2(d)) polarizations. At oblique incident angles, the symmetry of the square lattice is broken. For the TM polarization a transmission band opens up within the reflection band (Fig. 2(d)). This is caused by the splitting of the Fano resonance or guided resonance modes. As a result, the non-degenerate modes at Γ-point begin to become coupled to the incident radiation for increasing incident angles.[18,19] For the TM polarization a relatively narrower spectrum of 13 nm is reflected with high reflection (R > 95%). The TE polarized mode have less angle-dependent reflection properties, most likely related to the relatively-unchanged phase-matching conditions associated with the relatively flat modal dispersion properties.[20] TE polarized light reflects 1523 nm–1570 nm spectrum corresponding to a bandwidth of 47 nm for all incidence angles. The omni-directional reflection of this MR is limited by the incident angle dependent reflection of the TM polarization. Table I summarizes the simulated incident angle dependent reflection properties of the designed MR.

Detailed analysis of the angle dependent Fano resonant mode dispersion properties is presented in Fig. 3. Figs. 3(a) and 3(b) show the reflection and transmission spectra at

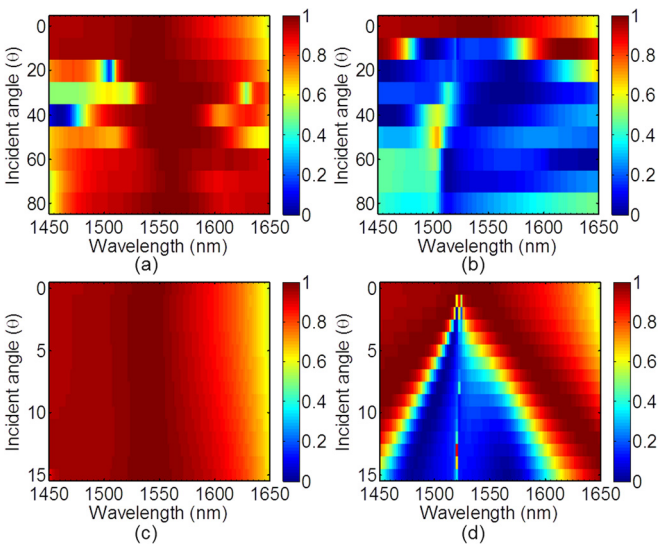

FIG. 2. (a) and (b) Contour plots of simulated reflectivity over a large range of incident angles θ (given in degrees) for (a) TE and (b) TM polarized light; and (c) and (d) Contour plots of simulated reflectivity for close to normal small incident angles θ (given in degrees) for (c) TE and (d) TM polarized light.

TABLE I. Simulated reflection characteristics of Si MR for different incidence angles for both TE and TM polarizations.

	Spectral range (nm)		Bandwidth (nm)	
Polarization type (Range of angles)	R > 90%	R > 95%	R > 90%	R > 95%
TE (0–80°)	1488–1586	1523–1570	98	47
TM (0–8°)	1386–1477	1461–1474	91	13
TE/TM (0°)	1388–1586	1472–1576	198	104

selected angles of $\theta = 0°$ and 5° for TE and TM polarizations, respectively. The reflection at surface normal incidence ($\theta = 0°$, $\Phi = 0°$) indicates the broadband nature of the Si MR. Following similar approach reported earlier,[5] the corresponding transmission spectra were plotted again in the logarithmic scale, as shown in Figs. 3(c) and 3(d). At surface normal incidence, two dominant guided mode resonances can be seen within the high reflection band where the transmission approaches zero. As the incident angle increases, more resonances are observed within the reflection band. To better understand the modal properties of these resonance modes, plane wave expansion method (PWE) was used to

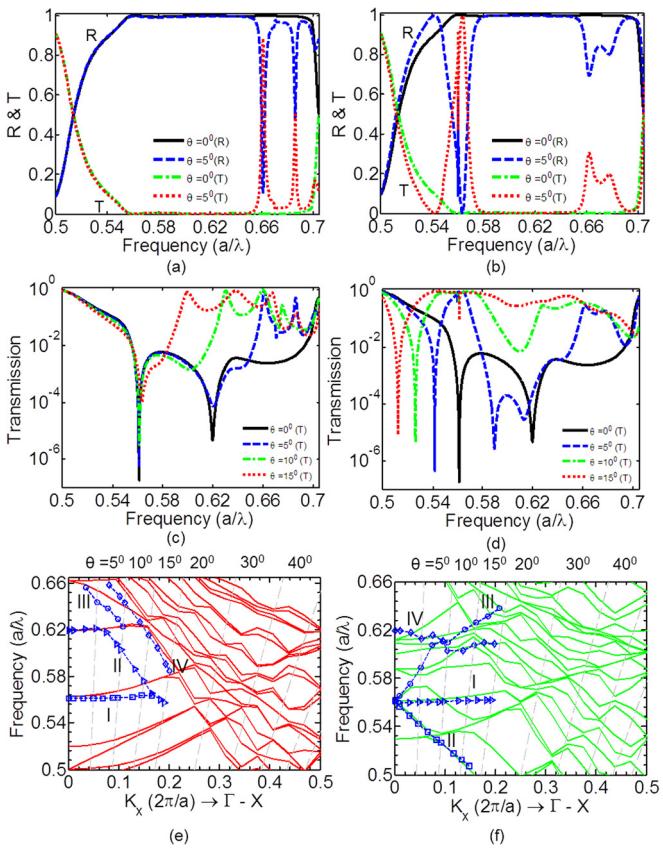

FIG. 3. (a) and (b) Simulated reflection and transmission spectra at different incident angles for (a) TE and (b) TM polarizations; (c) and (d) Simulated transmission spectra plotted in logarithmic scales showing locations of Fano resonances at various angles for (c) TE and (d) TM polarizations; and (e) and (f) Simulated dispersion plots for even (red) and odd (green) guided modes along (Γ–X) direction for (e) TE and (f) TM polarized light. The different markers represent the Fano resonance for various incident angles, identified from the simulated transmission spectra. The straight dashed gray lines represent the relationships between the normalized frequency and the normalized wave vectors along (Γ–X) direction. The bands labeled as I, II, III, and IV correspond to different Fano resonant modes.

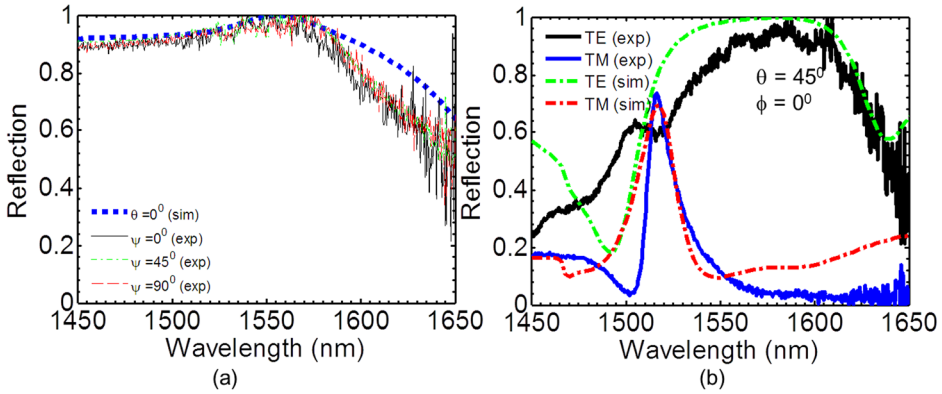

FIG. 4. (a) Simulated ("sim") and measured ("exp") reflection spectra at normal incidence ($\theta = 0°$) for various polarization (Ψ) angles; and (b) Simulated ("sim") and measured ("exp") reflection spectra for TE and TM polarized light incident at $\theta = 45°$ ($\Phi = 0°$).

compute the dispersion characteristics of the Si MR. The dispersion plot yields even and odd bands as shown in Figs. 3(e) and 3(f), respectively.[21] Considering the conventional definition of the Brillion zone symmetric points (Γ, X, and M) in the k-space (inset of Fig. 1(a)) and the incident angles (θ, Φ), the normalized frequency (a/λ) can be related to the normalized momentum $k_{\Gamma-X}$ in the dispersion plot as $k_{\Gamma-X} = (a/\lambda)\sin\theta\cos\Phi$, following a similar procedure reported earlier.[22] The identified Fano resonant modes from Figs. 3(c) and 3(d) are then mapped onto the dispersion plots, shown as the disconnected markers, corresponding to the resonance spectral locations under different incident angles. For the TE polarization, the dominant resonance mode (I) is relatively insensitive to the change of the incident angle within the range of 0° to 20°, which is responsible for a wide reflection band around this resonance (Fig. 2(c)). On the other hand, for the TM polarization, the dominant resonant mode (I) splits sharply into modes (I-III) with small changes in incident angles. This explains why the high reflection band at surface normal direction splits into two smaller reflection bands for higher incident angles (Fig. 2(d)). For both polarizations, with the increase of the incident angles, more higher order modes move into the reflection bands, which leads to drastic changes in reflection performances. With the control of the modal dispersion properties, the angle and polarization dependent reflection properties can be engineered for the desired applications.[6]

The simulation results were validated by characterizing the fabricated MR. The MR was fabricated on SOI substrate, based on standard e-beam lithography patterning technique and plasma dry-etching processes.[9,10] A broadband white light source is generated from a quartz tungsten halogen lamp that is collimated by a collimator. The beam is slightly focused (×4 lens) on the sample by the translational stage. The focused beam size is ~350 μm in diameter, much smaller than the 1 mm^2 patterned device area The reflected beam through the reflector was collected by the optical spectrum analyzer. The measured reflection spectrum was obtained by normalizing the measured reflection spectral intensity of the MR to that of the gold reference mirror. The polarization property was investigated by utilizing a Newport precision linear polarizer in our test set-up to control the incident beam polarization angle. For the surface normal incidence measurements, the polarizer was aligned along y-axis and x-axis for measuring TE and TM polarized light as shown in the schematic in Fig. 1. The incident beam polarization was swept from $\Psi = 0°$ to $\Psi = 90°$ for both TE and TM polarized beams. For oblique incidence measurements, the reflector was mounted at an angle of 45° with reference to the surface normal on an angle dependent stage. The Φ angle was changed by rotating the sample in the x-y plane. Care was taken to measure the reflection spectra for the Si MR at the same location and under the same conditions.

Fig. 4(a) shows the measured (denoted as "exp") and simulated (denoted as "sim") polarization dependent reflection spectra of the Si MR at surface normal incidence. The measured polarization independent reflection has a specular bandwidth of 180 nm (1400 nm–1580 nm)—greater than 90%. The high symmetry of the square lattice provides

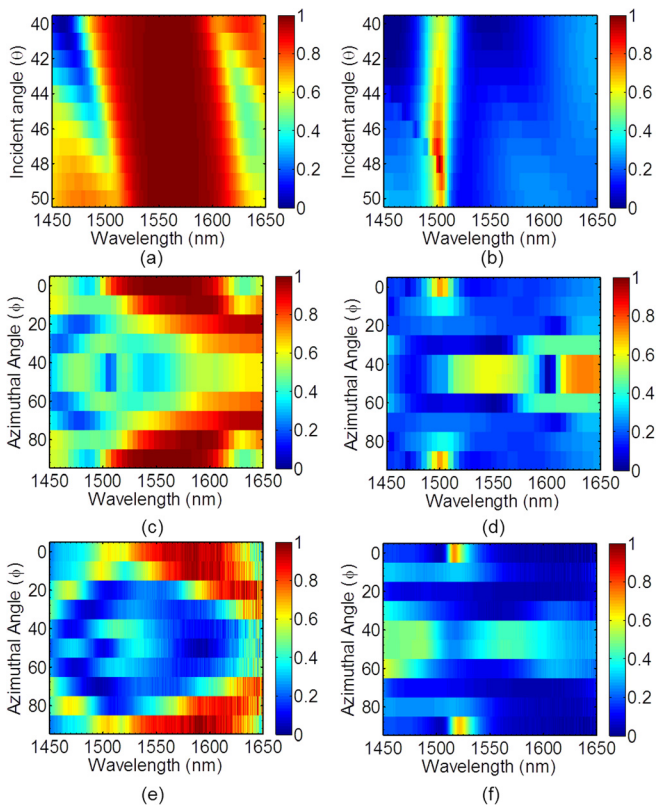

FIG. 5. Contour plots of simulated reflectivity of (a) TE (a) and (b) TM polarized light for a small range of incident angles close to an oblique incidence of $\theta = 45°$. Contour plots of simulated (c) and (d) and measured (e) and (f) reflectivity of the incident plane azimuthal angle Φ (given in degrees) for (c) and (e) TE and (d) and (f) TM polarized light at incident angle $\theta = 45°$.

TABLE II. Simulated reflection characteristics of Si MR for different polarization angles for TE polarization incident at 45°.

	Spectral range (nm)			Bandwidth (nm)		
Incident plane Azimuthal Angle (Φ)	R > 90%	R > 95%	R > 99%	R > 90%	R > 95%	R > 99%
0°	1516–1602	1523–1595	1542–1580	86	72	38
10°	1550–1611	1565–1606	–	61	51	–
15°	1580–1618	1598–1614	–	38	16	–
20°	1612–1664	1648–1654	–	52	6	–
30°	1696–1706	–	–	10	–	–
40°	1782–1801	1788–1793	–	19	5	–
45°	1755–1795	1760–1787	1766–1778	40	27	12

polarization independent broadband reflection for normal incidence, as seen in Fig. 4(a) the reflection spectra for different polarization angle $\Psi = 0°, 45°, 90°$. Fig. 4(b) shows the measured and simulated reflection spectra for TE and TM polarized light incident at $\theta = 45°$ ($\Phi = 0°$) on the Si MR. The measured reflection spectra agree qualitatively with the simulated results for both surface normal and oblique incidence light on the Si MR. With the polarization along the x-axis (Fig. 1(a)) of the lattice of the photonic crystal we see broadband reflection for TE polarization. We measured a 56 nm specular bandwidth for the TE polarization with reflectivity greater than 90%. A relatively low reflection is observed for the TM mode. An obvious question arises: What is the effect of incident plane azimuthal angle on the reflection of the Si MR?

Figs. 5(a) and 5(b) show relatively less variation in the simulated reflection of the Si MR for both the TE and TM polarizations for a range of angles close an oblique incidence (θ) of 45° ($\Phi = 0$). In other words, the testing of the mirror at an oblique incidence of 45° is quite tolerant to small incident angle misalignments. With the incident angle θ fixed at 45°, the impact of the incident plane azimuthal angle (Φ) was investigated. The simulated and measured reflection contour plots are shown in Fig. 5 at an oblique incidence, the symmetry of the square lattice is broken as seen by the TE and TM polarizations. As a result, the non-degenerate modes at Γ-point begin to become coupled to the incident radiation for increased incident angles.[23] A high degree of symmetry of the square lattice gives a symmetric response when the in-plane polarization angle changes from 0° to 90° for both the TE and TM polarizations. This symmetric response is verified experimentally for both the TE and TM polarizations. Table II summarizes the simulated TE polarization reflection characteristics of Si MR for different incident plane azimuthal angle incident at 45°. For TE polarization, this device remarkably achieves reflection (R > 90%) in an 86 nm wide band for light incident at 45°. When the incident plane is misaligned with reference to the one of the primary axis the reflection band shifts and reflectivity reduces. It is interesting to note that despite the azimuthal misalignment of the incident plane, this reflector still reflects TE polarization with reflectivity greater than 90% for 1580 nm–1602 nm spectrum with a 15° angular bandwidth. The angular tolerance can be increased at the expense of reduced bandwidth. An incident plane azimuthal misalignment shifts the spectral position of the reflection band and simultaneously reduces reflection at oblique incidence. The simulated bandwidth for the TE polarization changes from 86 nm to 40 nm when the incident plane azimuthal angle changes from 0° to 45°.

In conclusion, it is possible to achieve a high reflectivity from the Si MR at both surface normal and oblique angle incidences. A simulated 104 nm polarization independent specular bandwidth with reflection greater than 95% is easily achieved by the Si MR at surface normal incidence. We measured a specular bandwidth of 180 nm and 56 nm for the TE polarization at surface normal and oblique incidence of 45°, respectively, with reflection greater than 90%. The incident plane misalignment shifts the spectral position of the reflection band and simultaneously reduces reflection at oblique incidence. The experimental spectrum approximates the theoretical spectral response of this Si MR. The simulated specular bandwidth of the designed reflector is 86 nm and the measured bandwidth was found to be 56 nm for the TE polarization. For oblique incidence at 45°, the reflector provides greater than 90% reflection with a 30° incident plane angular tolerance and a 22 nm bandwidth for the TE polarization. The presence of the misalignment limits the use of the reflector where special spectral and polarization filtering is required. All the results can be helpful for such kind of reflectors into a wide range of photonic applications such as lasers, polarization dependent filters, optical interconnects, hollow core waveguides, beam splitters, coupled cavity systems, etc.

This work was supported by US AFOSR (FA9550-11-C-0026), ARO (W911NF-09-1-0505), and NSF (ECCS-1308520).

[1]C. F. R. Mateus, M. C. Y. Huang, L. Chen, C. J. Chang-Hasnain, and Y. Suzuki, IEEE Photon. Technol. Lett. **16**, 1676–1678 (2004).
[2]S. Boutami, B. Bakir, P. Regreny, J. Leclercq, and P. Viktorovitch, Electron. Lett. **43**, 282 (2007).
[3]M. C. Huang, Y. Zhou, and C. J. Chang-Hasnain, Nat. Photonics **1**(2), 119–122 (2007).
[4]Y. Ding and R. Magnusson, Opt. Express **12**(23), 5661–5674 (2004).
[5]R. Magnusson and M. Shokooh-Saremi, Opt. Express **16**(5), 3456–3462 (2008).
[6]V. Lousse, W. Suh, O. Kilic, S. Kim, O. Solgaard, and S. Fan, Opt. Express **12**(8), 1575–1582 (2004).
[7]S. Boutami, B. B. Bakir, H. Hattori, X. Letartre, J. L. Leclercq, P. Rojo-Romeo, M. Garrigues, C. Seassal, and P. Viktorovitch, IEEE Photon. Technol. Lett. **18**(7), 835–837 (2006).
[8]C. Sciancalepore, B. B. Bakir, X. Letartre, J. Harduin, N. Olivier, C. Seassal, J. Fedeli, and P. Viktorovitch, IEEE Photon. Technol. Lett. **24**(6), 455–457 (2012).

[9]H. Yang, S. Chuwongin, Z. Qiang, L. Chen, H. Pang, Z. Ma, and W. Zhou, Appl. Phys. Lett. **95**, 023110 (2009).
[10]H. Yang, D. Zhao, J. Seo, S. Kim, J. Rogers, Z. Ma, and W. Zhou, IEEE Photon. Technol. Lett. **24**(6), 476–478 (2012).
[11]H. Yang, D. Zhao, S. Chuwongin, J. H. Seo, W. Yang, Y. Shuai, J. Berggren, M. Hammar, Z. Ma, and W. Zhou, Nat. Photonics **6**(9), 615–620 (2012).
[12]D. Zhao, H. Yang, S. Chuwongin, J. H. Seo, Z. Ma, and W. Zhou, IEEE Photon. J. **4**(6), 2169–2175 (2012).
[13]C. J. Chang-Hasnain, Semicond. Sci. Technol. **26**, 014043 (2011).
[14]H. Wu, W. Mo, J. Hou, D. Gao, R. Hao, H. Jiang, R. Guo, W. Wu, and Z. Zhou, J. Opt. **12**, 045703 (2010).
[15]M. Shokooh-Saremi and R. Magnusson, Opt. Lett. **35**(8), 1121–1123 (2010).
[16]M. Kumar, C. Chase, V. Karagodsky, T. Sakaguchi, F. Koyama, and C. J. Chang-Hasnain, IEEE Photon. J. **1**(2), 135–143 (2009).
[17]M. G. Moharam and T. K. Gaylord, J. Opt. Soc. Am. **71**(7), 811–818 (1981).
[18]S. Fan and J. D. Joannopoulos, Phys. Rev. B **65**(23), 235112 (2002).
[19]S. Fan, W. Suh, and J. Joannopoulos, J. Opt. Soc. Am. A **20**(3), 569–572 (2003).
[20]W. Zhou, Z. Ma, H. Yang, Z. Qiang, G. Qin, H. Pang, L. Chen, W. Yang, S. Chuwongin, and D. Zhao, J. Phys. D **42**(23), 234007 (2009).
[21]S. G. Johnson, S. Fan, P. R. Villeneuve, J. Joannopoulos, and L. Kolodziejski, Phys. Rev. B **60**(8), 5751 (1999).
[22]Z. Qiang, H. Yang, L. Chen, H. Pang, Z. Ma, and W. Zhou, Appl. Phys. Lett. **93**(6), 061103–061106 (2008).
[23]K. Sakoda, *Optical Properties of Photonic Crystals* (Springer, 2005).